A Life Consumption Monitoring Methodology for Electronic Systems

Arun Ramakrishnan and Michael G. Pecht, *Fellow, IEEE*

***Abstract*—Failures in electronic products are often attributable to various combinations, intensities, and durations of environmental loads, such as temperature, humidity, vibration, and radiation. For many of the failure mechanisms in electronic products, there are models that relate environmental loads to the time to failure of the product. Thus, by monitoring the environment of a product over its life cycle, it may be possible to determine the amount of damage induced by various loads and predict when the product might fail.**

This paper describes the development of a physics-of-failure-based methodology for determining the damage or life consumption in a product. As a demonstration of the methodology, a data recorder has been used to monitor the temperature and vibration loads on a printed circuit board placed under the hood of a car. The data collected by the recorder has been used to determine the life consumption in the solder joints of the printed circuit board due to temperature and vibration loading. The calculated remaining life has then been compared with temperature cycling test results on the board to assess the validity of the approach.

***Index Terms*—Humidity, life consumption, physics-of-failure, printed circuit board, radiation, temperature cycling, vibration.**

I. Introduction

A PRODUCT'S health is the extent of its degradation or deviation from its normal operating state. Health monitoring is a method for evaluating a product's health as a means to determine whether and when failure will occur. The goal of health monitoring is to [1].

1) Reduce lost output penalties.
2) Reduce forced outage repair and labor costs.
3) Reduce spares holdings.
4) Reduce frequency of failures.
5) Improve safety margins.
6) Reduce insurance premiums.
7) Extend maintenance cycles.
8) Maintain the effectiveness of equipment through timely repair actions.
9) Improve repair quality.
10) Increase profitability.
11) Help in the design of future products.

A product's health can be determined in two ways, i.e., condition monitoring and life consumption monitoring. The purpose of determining product health is to quantify the amount of product degradation, and hence to support decisions related to the operation and maintenance of the product.

Condition monitoring is a method of evaluating a product's current operating state. An example of condition monitoring is Boeing's extended-range twin-engine operations (ETOPS) program [2]. Two typical examples of the ETOPS program are engine condition monitoring (ECM) and oil consumption monitoring. ETOPS operators are required to use ECM programs to monitor adverse trends in engine performance and execute maintenance to avoid serious failures (e.g., events that could cause in-flight shutdowns, diversions, or turnbacks). The ECM programs monitor engine parameters such as exhaust temperature, fuel and oil pressures, and vibration. In some cases, oil consumption data and ECM data are combined to identify problems in normal engine operation [2]. Built-in-test (BIT) [3] concepts and "smart" sensors [4] are also employed for interruptive and/or continuous monitoring of electronic systems.

Life consumption monitoring is a process that involves the continuous or periodic measurement, sensing, recording, and interpretation of physical parameters associated with a product's life cycle environment to assess or predict remaining life. This paper will focus on the life consumption monitoring methodology.

II. Life Consumption Monitoring Methodology

The growing demand for improvements in product reliability is universal at a time when product complexity is rapidly escalating. In addition, people are becoming more interested in predicting the field reliability and operational availability of their products, along with the various factors that can affect reliability.

A life consumption monitoring methodology for a product (see Fig. 1) consists of three steps: monitoring critical parameters of the product's life cycle environment, simplification of the monitored data, and physics-of-failure analysis. Monitoring the critical parameters of the product's life cycle environment involves the periodic measurement of the loads critical to the reliability of the product. Data simplification involves conversion of the monitored data into a form compatible with the input requirements of reliability assessment models. Physics-of-failure analysis involves the determination of the cumulative damage[1] accumulation in the product due to various failure mechanisms induced by the monitored loads. Each of these steps is discussed in the sections to follow.

Manuscript received September 1, 2002; revised January 12, 2003. This work was recommended for publication by Associate Editor B. Courtois upon evaluation of the reviewers' comments.

M. G. Pecht is with the CALCE Electronic Products and Systems Center, University of Maryland, College Park, MD 20742 USA.

A. Ramakrishnan is with LSI Logic Corporation, Milpitas, CA 95035 USA.

Digital Object Identifier 10.1109/TCAPT.2003.817654

[1]Damage is defined as the extent of a part or product's degradation or deviation from its normal operating state.

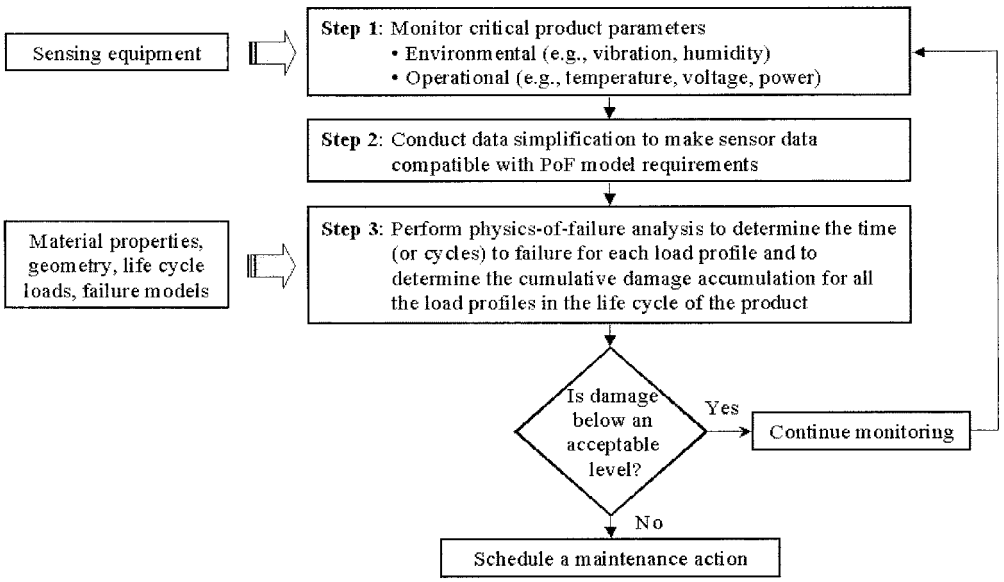

Fig. 1. Various steps involved in a life consumption monitoring methodology.

A. Monitoring Critical Parameters of a Product's Life Cycle Environment

The life cycle environment of a product consists of the assembly, storage, handling, and use of the product (application and operational loads), including the severity and duration of these conditions [5]. Specific life cycle loads include environmental conditions such as temperature, humidity, pressure, vibration or shock, chemical environments, radiation, contaminants, and loads due to operating conditions, such as current, voltage, and power. These loads may affect the reliability of the product either individually or in combination with each other. The selection of the load parameters to be monitored depends on various factors, such as the monitoring methods available to the user [6], the type of failure mode or failure mechanism the user is concerned with[2], the conditions that precipitate these failure modes, and the inputs required by the failure models used for assessing the reliability of the product.

B. Data Simplification

Almost all monitoring systems use sensors to measure the various loads present in a product's environment. A sensor is a device that provides, in most cases, a usable electrical output signal in response to a specified measurand. For life consumption monitoring, sensor data must usually be simplified to make it compatible with the input requirements of the selected reliability prediction models. Two methods used for data simplification are discussed in this section.

1) Data Reduction: Data reduction is useful in life consumption monitoring to reduce data storage space and to reduce the time for damage calculations. By using information that is most relevant to the failure models, an efficient data reduction method should [7].

1) Permit gains in computing speed and testing time.
2) Condense load histories without sacrificing important damage characteristics.
3) Preserve the sequence of any damaging reversals[3] in the original loading
4) Provide an estimate of the error introduced.

The ordered overall range (OOR) method, which satisfies all of the above criteria, provides a technique to convert an irregular history into a regular sequence of peaks and valleys and also allows the user to specify the range (i.e., upper limit—lower limit) of the reversals to be eliminated. A screening level[4] is used to define the range of the reversals to be eliminated.

The OOR method can be described by imagining a car traveling along a course from west to east (see Fig. 2), taking the shortest possible route through the course [7]. Each location where the car changes its direction from north to south (or vice versa) is marked by a flag, and corresponding reversals in the original loading sequence are noted. Peaks and valleys that were originally separated by smaller interrupting ranges now become adjacent, creating larger overall ranges. This allows smaller load fluctuations to be screened out while preserving the sequence of the most damaging reversals.

The OOR method can also be applied to a load history by selecting one of the extreme reversals in the history (either the largest peak or the smallest valley), and choosing the next reversal that differs from the selected reversal by more than the screening level as the first tentative candidate. The approach for selecting the tentative candidate is as follows [7], [8].

— If the selected starting reversal is a peak, the next valley that differs by more than the screening level from the

[2]If the user has prior knowledge of the product's environment, then techniques such as failure mode, effects and criticality analysis (FMECA) or physics-of-failure analysis (performed using the expected environment) can be used to determine the likely failure mechanisms in the product, which in turn can be used to select the environmental parameters to be monitored.

[3]A reversal is defined as the point at which the first derivative of the time history changes sign. A reversal can either be a peak (where the first derivative changes from a positive to a negative sign) or a valley (where the first derivative changes from a negative to a positive sign).

[4]The screening level is a fraction of the maximum range (i.e., largest peak—smallest valley) in the history.

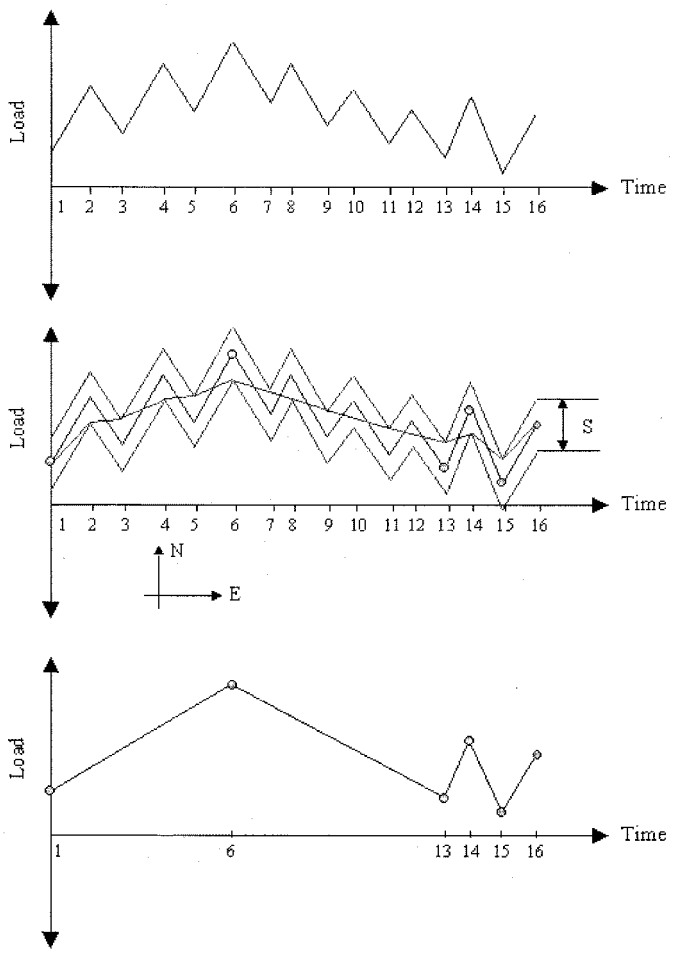

Fig. 2. Application of the OOR method. The first figure shows the original load history. The second figure shows the "car" traversing the shortest route through the course, with each point where the car changes direction being counted. The last figure shows the reduced profile, consisting only of the points counted in the previous step [7].

peak is selected as the first tentative candidate. Succeeding reversals are then checked. Peaks are checked to see if they differ from the candidate by more than the screening level (event "x"), and valleys are checked to see if they are lower than the candidate (event "y"). If event "y" occurs first (i.e., before event "x"), then the candidate is rejected and the new valley becomes a candidate. If event "x" occurs first, the candidate is validated and the newly found peak becomes the next candidate.

— If the selected starting reversal is a valley, the next peak that differs by more than the screening level from the peak is selected as the first tentative candidate. Succeeding reversals are then checked. Valleys are checked to see if they differ from the candidate by more than the screening level (event "x"), and peaks are checked to see if they are higher than the candidate (event "y"). If event "y" occurs first (before event "x"), then the candidate is rejected and the new peak becomes a candidate. If event "x" occurs first, the candidate is validated and the newly found valley becomes the next candidate.

This process continues until the last reversal is counted. Since the counting process starts from an extreme reversal (which may or may not be the first reversal in the history), the method has to be applied to both sides of the starting reversal to take the entire load history into account.

2) Cycle Counting: Cycle counting methods are used to transform a time history consisting of several reversals (peaks and valleys) into an equivalent cyclic history [9]. The rainflow counting method has been used in this paper to count cycles. In the rainflow method, the load-time history is plotted with the time axis vertically downward, and the lines connecting the load peaks consistent with a series of sloping roofs [10]. The rain flow is initiated by placing drops successively inside each reversal. Cycles and half cycles are identified by imposing rules on the rain dripping down the roofs [9].

a) The rain is allowed to flow on the roof and drip down to the next slope except that, if it initiates at a valley, it must be terminated when it comes opposite a valley equal to or more negative than the valley from which it initiated. A half cycle is then defined between the starting valley and the next peak.
b) Similarly, if the rain flow is initiated at a peak, it must be terminated when it comes opposite a peak equal to or more positive than the peak from which it initiated. A half cycle is then counted between the starting peak and the next valley.
c) The rain flow must also stop if it meets rain from a roof above. This ensures that every part of the load history is counted once and only once.
d) Cycles are counted when a counted range can be paired with a subsequent range of equal magnitude in the opposite direction.

The rainflow method does not provide any information about the mean load or the time taken for the load to increase from its peak to its valley (and vice versa). A modified method called three-parameter rainflow cycle counting has been used to handle this situation [11]. This method accepts a sequence of successive differences between peak and valley values (P/V ranges) in the time history as an input, and determines the range of the cycle, the mean of the cycle, and the half-cycle time. The dwell time at the extremes of the cycle is assumed to be 25% of the half-cycle time. The modified method identifies cycles as follows [12]. Consider three successive P/V differences d_1, d_2, and d_3, as shown in Fig. 3. A cycle is identified only if the following condition is true:

$$d_1 > d_2 \leq d_3. \tag{1}$$

The condition of (1) is called the 'loop condition.' For a given sequence of P/V ranges, if the loop condition exists, the method picks the loop corresponding to size d_2 off the cycle, leaving only the residual wave 1-2-4-5, corresponding to a half-loop size $(d_3 - d_2 + d_1)$ in the load plot. This operation is called 'loop-reaping.'

For a given sequence of P/V ranges, the three-parameter rainflow method "reaps" the smaller cycles that occur during a larger cycle. The range, mean, and half-cycle time of the residual half cycle is adjusted according to the loop-reaping

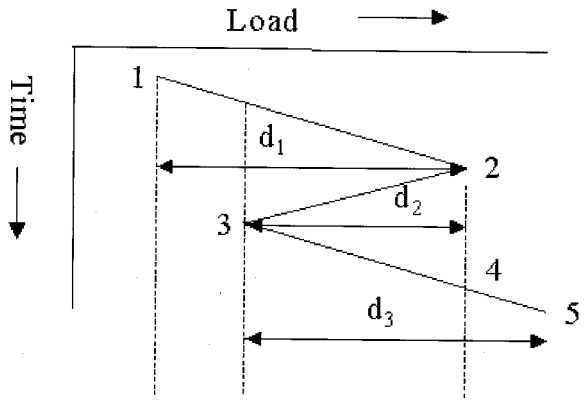

Fig. 3. Loop condition and loop reaping operations [12]. Cycles are identified only when the magnitude of the second range (d_2) lies between the first (d_1) and the third (d_3). When this happens, the three-parameter rainflow method stores the cycle with the range d_2 into a buffer, and updates the load history with a single half-cycle of range $(d_3 - d_2 + d_1)$.

condition, and the process is applied until the last P/V range is read. The counted cycles and residual half-cycles are placed in separate arrays that store the cyclic range, the cyclic mean, and the time taken to complete the half cycle.

C. Physics-of-Failure Analysis

The objective of a physics-of-failure analysis in the life consumption monitoring process is to determine the cumulative damage accumulation due to various failure mechanisms for a product in a given environment. A physics-of-failure analysis consists of design capture, identification of potential failure modes, mechanisms, and sites, and reliability assessment.

Design capture is the process of collecting geometrical (dimensional) and material information about a product to generate a model of the product. This step involves characterizing the product at all levels—parts, circuit cards, enclosures, as well as physical interfaces. Design data (such as material properties, power dissipation, mechanical and electrical properties, and part geometry) can either be obtained directly from the manufacturer or by making reasonable assumptions based on measurements or experience.

Identification of potential failure modes, mechanisms, and sites involves using the geometry and material properties of the product together with the measured life cycle loads acting on the product to identify the potential failure mechanisms,[5] failure sites[6] (e.g., part interconnects, board metallization, and external connections), and failure modes[7] (e.g., electrical shorts or opens) in the product. This task may involve a failure modes and effects analysis (FMEA) and a simulation-based methodology.

Reliability assessment involves determining the life of the product for a particular failure mechanism and operating conditions, and using the life of the product and the life cycle loads to determine the total damage accumulation in the product.

It is necessary to select the appropriate physics-of-failure models for the previously identified failure mechanisms, and use the material properties, product geometry, and life cycle loads to conduct a load-stress analysis (i.e., compute the stress profile) on the product. The computed stress is then used to determine the life of the product (e.g., time to failure, cycles to failure) for the particular failure mechanism and operating conditions.

The basis of damage assessment is that operation of a part at a given stress amplitude will produce some amount of damage in the part, the magnitude of which will be related to the total time of operation at that stress amplitude and the total time that would be required to produce failure of an undamaged part at that stress amplitude [9]. The damage induced is assumed to be permanent, and operation at several different stress amplitudes in sequence is assumed to result in an accumulation of total damage equal to the sum of the damage increments accrued at each individual stress level [9]. When the total accumulated damage reaches a critical level, failure is predicted to occur.

Many models have been proposed for quantifying damage caused by operation at a given stress level and for adding damage increments to predict failure under multi-loading conditions. The Palmgren–Miner cumulative damage theory or the linear damage theory is used in this paper [13].

The Palmgren–Miner theory can be explained as follows. Let operation at a constant stress amplitude S_1 produce complete damage in a part (100%) in N_1 cycles. Hence, operation at the same stress amplitude S_1 for a number of cycles n_1 smaller than N_1 will produce a smaller fraction of damage, say D_1. If the stress profile for the part includes many stress levels, a damage fraction D_i will be produced for each of the different stress levels S_i in the spectrum.

The Palmgren–Miner theory states that the damage fraction (D_i) at any stress level S_i is linearly proportional to the ratio of the number of cycles of operation (n_i) to the total number of cycles that would produce failure (N_i) at that stress level. In other words

$$D_i = \frac{n_i}{N_i} \tag{2}$$

and failure is expected to occur if

$$\sum D_i = \sum_{j=1}^{i} \frac{n_j}{N_j} \geq 1. \tag{3}$$

Neglecting any hysteresis and transient effects in a time-varying environment, the Palmgren–Miner theory can be expressed in terms of time-to-failure and time of operation at a given stress level as

$$D_i = \frac{t_i}{\mathrm{TTF}_i} \tag{4}$$

where t_i is the number of cycles of operation at stress S_i and TTF_i is the number of cycles to failure at the same stress S_i.

[5]A failure mechanism is a process (such as creep, fatigue, or wear) through which a defect nucleates and grows as a function of stresses (such as thermal, mechanical, electromagnetic, or chemical), ultimately resulting in the degradation or failure of a product.

[6]A failure site is the location of the failure.

[7]A failure mode is a physically observable change caused by a failure mechanism.

The Palmgren-Miner theory has two shortcomings:

1) it does not recognize the influence of the order of application (i.e., sequence) of the various stress levels;
2) it does not capture the influence of stress levels on the damage accumulation rate.

Damage is assumed to accumulate at the same rate at a given stress level without regard to past history, although experimental results have shown that damage can accumulate in a nonlinear manner. As a result, many nonlinear damage theories have been proposed to account for the nonlinearity in damage accumulation, and several researchers have reviewed, evaluated, and compared the various cumulative damage accumulation theories available [14]. In general, Miner's rule is recommended for its simplicity, versatility, and reasonable accuracy [15].

D. Acceptable Limit of Damage Accumulation

The life consumption monitoring methodology concludes with the calculation of the total damage accumulation in the product. At this point, the user is presented with a choice: to decide whether to keep the product in operation and continue monitoring or to decide that the product is approaching an unacceptable level of performance and schedule a maintenance action. The choice of the acceptable limit of damage depends on a variety of factors, such as the user's application and the safety level associated with it, the type of failure the user is interested in, and the user's definition of failure. For example, if the application involves human participation (such as aircraft or spacecraft) or may compromise the safety of personnel (such as machinery in a factory), a lower limit of damage accumulation may be chosen, but if the application is known to be fairly reliable (such as systems with multiple redundancy), a higher limit of damage accumulation may be selected.

III. Demonstration of the Life Consumption Monitoring Methodology

The methodology described in this paper and shown in Fig. 1 was demonstrated in a real-time environment through an experiment, which involved the following steps.

1) Mounting a printed circuit board (PCB) under the hood of a car.
2) Monitoring the thermal and vibration underhood environment of the PCB while it stayed in the car.
3) Simplifying the monitored environment for solder joint fatigue analysis and performing a physics-of-failure-based reliability analysis to determine the life consumption of the solder joints for the duration the PCB stayed in the car.
4) Predicting the remaining life (in terms of cycles to failure) of the solder joints if the PCB is only thermally cycled for the remainder of its life.
5) Determining the actual remaining life of the solder joints by thermally cycling the PCB to failure.
6) Comparing the predicted and the actual remaining life results.

The PCB used for the experiment contained 8 leadless inductors, each soldered with eutectic solder to an FR-4 substrate. The operating temperature range of the inductors was -55 to 125 °C. The PCB was mounted on the exhaust manifold of a 1995 Eagle Talon. Two aluminum strips were bolted to the exhaust manifold, and two holes were tapped in each of the aluminum strips for holding the PCB in place. This arrangement allowed the corners of the PCB to be modeled as simple point supports in the reliability analysis.

A self-powered data-recording device equipped with a triaxial accelerometer and an integrated temperature and humidity sensor was used to record the environment of the PCB at programmed intervals. The data recorder was capable of recording two types of data: dynamic (i.e., data that varies rapidly with time) and static (data that can be completely characterized by a single reading). In order to prevent any overlapping of dynamic and static data, the recorder's memory (8 MB) was divided into two partitions.

1) *Signal-triggered*: This allows the user to specify the minimum value of a parameter that should be exceeded before the parameter recording begins. This feature is primarily for measuring dynamic data.
2) *Time-triggered*: This allows the user to specify the minimum time interval to elapse before recording begins. This feature is primarily for measuring static data.

The user selects the frequency range and the number of analysis lines for dynamic data analysis, which is used to fix the sampling rate (i.e., the number of samples counted per second) and the sample size (i.e., the number of samples per record). A low-pass filter was used to screen out all frequencies above the Nyquist frequency to prevent aliasing. The frequency of the low-pass filter was set to 40% of the sampling rate [8] [16].

The data recorder could not be placed directly under the hood of a car because its internal sensors had a maximum operating temperature of 55 °C, and its size and weight precluded its installation anywhere under the hood. As a result, the data recorder was kept under the passenger seat of the car, and external sensors were used to monitor the vibration and thermal [17] environment of the PCB.

The data recorder (see Fig. 4) had eight dynamic channels and six static channels for recording data, of which three dynamic channels were dedicated to the internal accelerometer and two static channels were reserved for the internal temperature and humidity sensor. One of the five remaining dynamic channels could be used for an external accelerometer, and two of the remaining four static channels could be used for an external temperature and humidity sensor. In our experiment, one external single-axis accelerometer[9] and one external temper-

[8]Sampling theory states that if a signal is sampled such that the time interval between adjacent sampling points is h seconds (or the sampling rate is $1/h$), then the maximum frequency that can be measured is $1/2h$ (called the Nyquist frequency), and any frequency component above $1/2h$ contained in the original signal will be superimposed or "aliased" back into the frequency range from 0 to $1/2h$. Hence, it is required that all frequencies above $1/2h$ be eliminated from the original signal. This also follows from Shannon/Nyquist's theorem—the sampling rate $(1/h)$ has to be at least twice the absolute maximum frequency of the original signal $(1/2h)$ in order to reconstruct the original signal.
The common way to ensure that the absolute maximum frequency of the original signal stays below $1/2h$ is to use a low-pass filter circuit, which only allows signals lower than the filter frequency to pass through. An ideal filter should hence be set to 50% of the sampling rate (i.e., 50% of $1/h = 1/2h$). The data recorder's nonideal filter is set to 40% of the sampling rate to ensure that it will screen out all frequencies above $1/2h$.

[9]The chosen axis of vibration was the z-direction.

ature sensor were used for monitoring the vibration and temperature in the car. The acceleration sensor used for the experiment was a single-axis piezoelectric sensor and the temperature sensor was a resistance thermo-detector (RTD). Both sensors were calibrated with the data recorder's internal sensors after installation.

Given the maximum frequency of interest and the number of analysis lines in the power spectral density (PSD) plot, the data recorder calculates the sampling rate and the sample size for signal-triggered analysis according to the following equations [16]:

$$\text{Maximum frequency of interest (Hz)} = \frac{\text{Sampling rate } \left(\frac{\text{samples}}{\text{second}}\right)}{2.56} \quad (5)$$

and

$$\text{Number of analysis lines} = \frac{\text{Sample size } (N)}{2.56}. \quad (6)$$

In order to select the maximum frequency of interest, the data recorder was first programmed to collect data at its highest sampling rate[10] (3072 samples/sec, which corresponds to a maximum measurable frequency of 1200 Hz), and the resulting frequency spectrum was analyzed. It was observed that the PSD of the vibrations was concentrated around 70–200 Hz and the PSD was negligible above 600 Hz. Hence, the frequency analysis range was conservatively selected to be 1 to 700 Hz to save memory. The number of analysis lines was selected to be 400 (the maximum) for highest resolution. The sampling rate and the sample size were thus set at 1800 samples per second and 1024 respectively. The corresponding time interval between two sample values ($h = 1$/sampling rate) was 0.55 msec and the total record length ($T = \mathrm{Nh}$) was 568 ms.

We monitored only two loads in the car: temperature and vibration. The effect of the other environmental parameters (such as humidity, chemicals, and radiation) was ignored. The reasons for ignoring the effect of the other parameters were as follows.

- The test board was designed so that the solder joints connecting the inductors to the board would be the first components of the board to fail. Also, CALCE's experience in solder joint fatigue indicated that of all the environmental variables under the hood of a car, only vibration and temperature would induce solder joint fatigue
- We did not possess the necessary sensing equipment that were compatible with the data recorder for monitoring any other variables

The vibration sensor was glued to one of the aluminum strips near one of the screws, and the temperature sensor was taped to the surface of the PCB, as shown in Fig. 5. The road vibrations were transmitted to the PCB through the screws, and the heat carried by the exhaust gases was transmitted to the PCB via conduction through the screws and natural convection through the air between the exhaust manifold and the PCB. We recorded the temperature and vibration environment of the PCB for five days in February in College Park, MD. The data was downloaded for analysis at regular intervals. The process followed for characterizing temperature and vibration is described in Sections III-A–D.

[10]This was done to find the frequency range of interest and to ensure that any high-frequency vibrations would not be eliminated in the actual experiment.

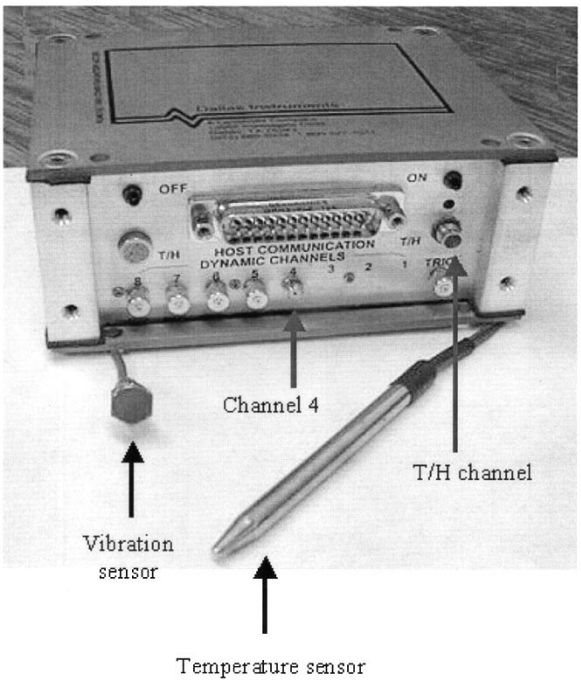

Fig. 4. Data recorder with the external temperature and vibration sensors. The temperature sensor was connected to the T/H channel and the vibration sensor was connected to Channel 4.

A. Temperature Characterization

Initial experiments were carried out to determine the temperature extremes on various locations in the car before actually placing the PCB in the car. The temperature of the exhaust manifold surface was measured to be 157 °C. Since an FR-4 PCB has a glass transition temperature between 125–135 °C and the inductors were rated only up to 125 °C, the PCB was placed near, but not directly on the exhaust manifold surface. Aluminum strips were used to provide an air gap between the exhaust manifold and the PCB, allowing natural convection to reduce the temperature of the PCB below 125 °C.

Fig. 6 shows the temperature profile on the exhaust manifold over four days. Each data point was taken at an interval of 10 min (i.e., the time trigger was set to 10 min). The figure shows that the maximum temperature seen by the PCB was 120.5 °C, which is lower than the glass transition temperature of the FR-4 board as well as the rated temperature limit of the inductors.

The temperature versus time history for the three days was converted into an equivalent sequence of peaks and valleys (for thermal fatigue analysis) using the OOR method. Fig. 7 shows the results of the OOR algorithm (with a screening level of zero) on the temperature data in Fig. 6. The peak-valley difference (P/V) sequence generated by the OOR algorithm was then given as an input to the three-parameter rainflow cycle counting algorithm. The cycles and half-cycles counted by the algorithm were used as an input for the physics-of-failure analysis.

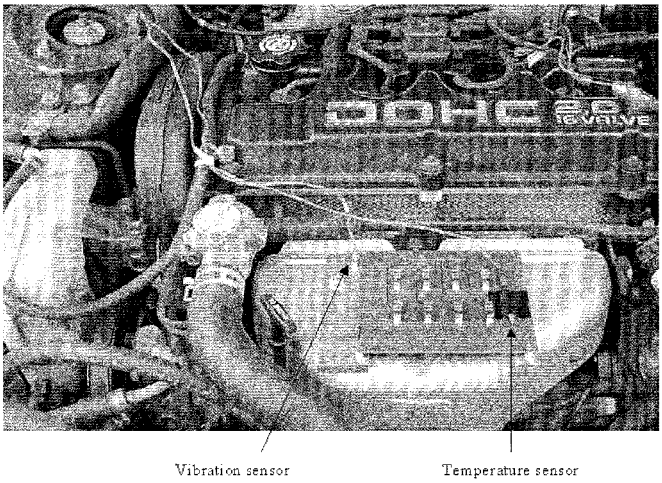

Fig. 5. Location of the temperature and vibration sensors in the car. The PCB was mounted on the exhaust manifold of the car using two aluminum strips.

B. Vibration Characterization

Vibration was measured as a signal-triggered quantity, i.e., vibration data was recorded when the magnitude of the vibration exceeded the preset trigger. In order to find the appropriate trigger for the experiment, trials were conducted to find the time it took to fill the recorder's memory reserved for dynamic analysis with various trigger values[11]. Based on the results, the vibration trigger was set as ± 6.5 g for the experiment.[12]

Since the vibration experienced in a car is random (i.e., it cannot be described by an explicit mathematical relationship), its intensity was described in terms of its power spectral density (PSD). The PSD describes the frequency composition of the vibration in terms of its mean square value over a frequency range. The mean square value of a time history $x(t)$ in a frequency range between f and $f + \Delta f$ sampled over a record length T is given by [18]

$$\Psi^2(f, \Delta f) = \lim_{T \to \infty} \frac{1}{T} \int_0^T x^2(t, f, \Delta f)\, dt \tag{7}$$

where $x(t, f, \Delta f)$ is that portion of $x(t)$ that is in the frequency range from f to $f + \Delta f$. For small Δf, the PSD function is defined as [18]

$$G(f) = \lim_{\Delta f \to 0} \frac{1}{\Delta f} \left[\lim_{T \to \infty} \frac{1}{T} \int_0^T x^2(t, f, \Delta f)\, dt \right]. \tag{8}$$

For sampled data (i.e., the type of data recorded in this study), the PSD is calculated by the Cooley–Tukey method, which is based on computing the PSD via a fast Fourier transform (FFT) of the original sampled acceleration data. This method can only be applied if the sample size is a power of two. For a sequence of acceleration values h_k sampled over a record length T, the Cooley-Tukey method defines the PSD function at any frequency f as [18]

$$G(f) = \frac{2h}{N} |X_k|^2 \tag{9}$$

where X_k are the FFT components of the N sampled acceleration values of amplitude h_k averaged over the record length T. The expression for finding X_k is given by [19]

$$X_k(n) = \sum_{k=0}^{N-1} h_k e^{i(2\pi kN/n)} \tag{10}$$

where N is the sample size and is a power of two. The independent variable n can be related to the frequency by the relation $f_n = (n/Nh)$, where h is the sampling interval between adjacent points and T is the total record length.

The bandwidth Δf over which the PSD is displayed is calculated according to the formula

$$\Delta f = \frac{\text{Sampling Rate}}{\text{Sample Size}}. \tag{11}$$

The software used in this experiment for assessing the reliability of the solder joints takes PSD and frequency data as an input for vibration analysis, so this form of data is desirable. Fig. 8 shows the PSD curve (averaged over the record length T) for the excitation given to the PCB over four days.

C. Damage Assessment in the Car

The life consumption in the solder joints of the PCB due to temperature and vibration loading in the car was determined using calcePWA.[13] The software conducts a physics-of-failure analysis and calculates cumulative damage according to the Palmgren-Miner rule. The properties of the PCB (i.e., number of layers, dimensions) and the solder joint dimensions were obtained from the PCB manufacturer, and the output of the three-parameter rainflow cycle counting algorithm and the PSD versus frequency data were used to find the damage fractions for the temperature and vibration loading in the car.

The boundary conditions used in the damage assessment were as follows:

1) the corners of the PCB were modeled as simple point supports for the vibration analysis;
2) the edges of the PCB were set to the measured temperature, and conduction with natural convection was used to find the thermal profile on the PCB.

The thermal gradient in the PCB was found to be very small ($\sim 0.06\,^{\circ}\mathrm{C}$) due to the absence of any significant on-board heat sources.

The boundary conditions assumed for the vibration analysis were verified by comparing the natural frequencies of the PCB with the values predicted by calcePWA. The calcePWA vibration analysis had predicted that the natural frequencies of the PCB were 85, 179, 260, and 459 Hz, respectively. To check this, the mode shapes of the PCB for these frequencies were analyzed and the external accelerometer was mounted on the PCB

[11]99% of the data recorder's 8 MB memory was reserved for vibration measurement, and 1% for temperature measurement. This memory partition ratio was maintained for all trials during the course of this experiment.

[12]The trigger value corresponds to the instantaneous value of the induced vibration at any point in the record length (568 ms). In other words, if the sensor detects that the instantaneous vibration exceeds the 6.5 g value at any point in the 1024 sampling points per record, it saves the entire record. The average vibration for the entire record is, of course, much smaller.

[13]calcePWA is a reliability assessment software developed by the CALCE Electronic Products and Systems Center.

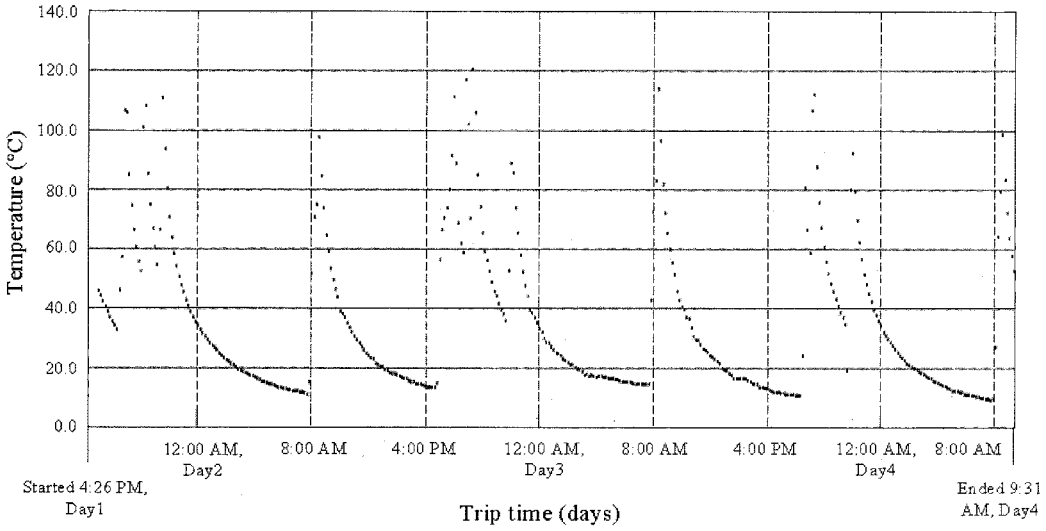

Fig. 6. Temperature profile on the exhaust manifold as measured by the data recorder. Each data point is taken at an interval of 10 min.

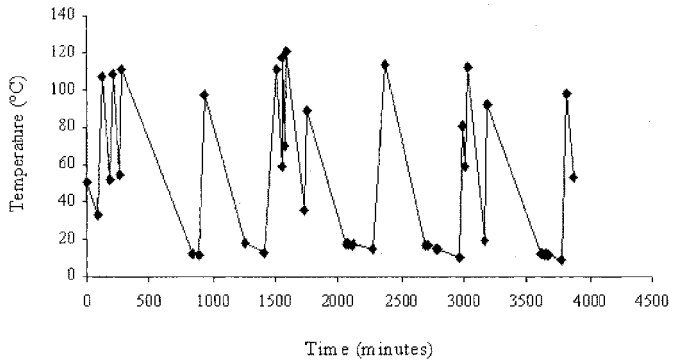

Fig. 7. Temperature profile after OOR reduction. A comparison of this plot with Fig. 6 shows that the OOR method has only captured the end points of the various temperature ranges from the original history.

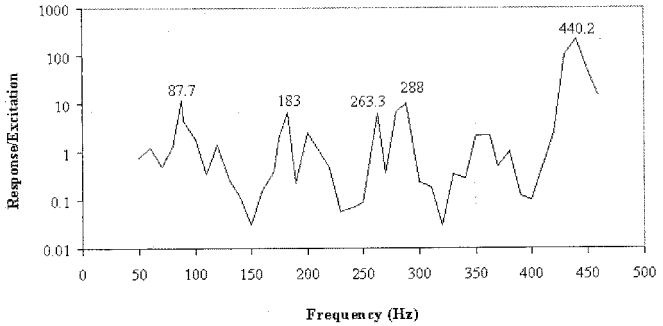

Fig. 9. Plot of the ratio of the PCB response to PCB excitation (both in PSD) against frequency. The peaks in this plot identify the natural frequencies of the PCB. The frequencies corresponding to the peaks are shown above the respective peaks.

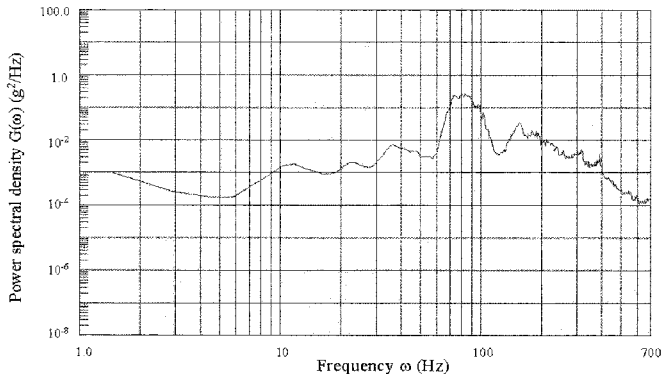

Fig. 8. PSD versus frequency plot for the vibration in the car. The figure shows that most of the energy of the road vibration is centered around a frequency of 80 Hz.

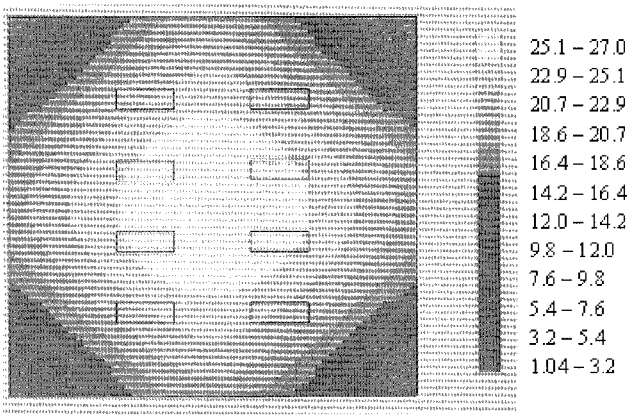

Fig. 10. Displacement contours on the PCB for the first mode of vibration. All dimensions are in mils. The calcePWA analysis predicted that most of the damage occurs in the first mode of vibration, in which the inductors in the center of the board see a larger curvature.

at a location that always had a nonzero displacement. The response of the PCB to the driving conditions was then measured, and the ratio of the response of the PCB to the excitation given to the PCB at various frequencies was plotted against the frequency. Any peaks in this plot would identify the actual natural frequencies of the PCB during the experiment. As Fig. 9 shows, the natural frequencies occur at 87, 183, 288, and 440 Hz, which is in agreement with the calcePWA prediction. Also, the first observed natural frequency (87 Hz) is close to the frequency with highest PSD value (80 Hz—see Fig. 8), which suggests that the board is likely to experience maximum curvature in its first

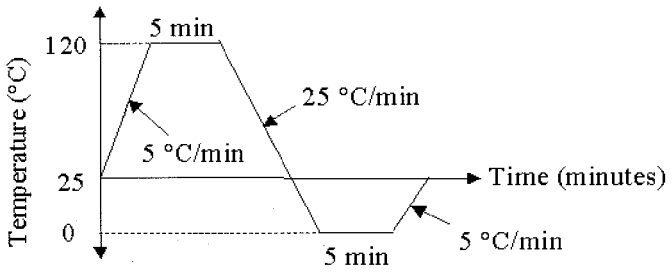

Fig. 11. Profile used for the temperature cycling test.

mode shape, and consequently accumulate the largest damage in that mode shape.

The calcePWA damage analysis predicted that the inductors in the center of the PCB see a larger curvature, and hence accumulate greater damage than the inductors in the periphery (see Fig. 10).[14] The average damage accumulation in the solder joints was predicted to be 0.53,[15] which meant that an average of 47% of the solder joints' life was still remaining.

D. Verification of Remaining Life

An accelerated temperature cycling test (the profile is shown in Fig. 11) was selected to use up the remaining life of the solder joints.[16] The calcePWA software was used to find the number of cycles required to consume the remaining life of the solder joints (i.e., a life consumption of 47%) for the given temperature profile, which worked out to 52 cycles.

In order to verify the life consumption predicted by calcePWA, the PCB from the car was subjected to the same accelerated temperature cycling test. All inductors were monitored real-time with an ANATECH event detector which recorded transient electrical opens (called "events") for each inductor. The resistance of each inductor was measured prior to the test and monitored during the test. The threshold resistance of the event detector was set to 126 Ω, and a "failure" was classified as the occurrence of fifteen events (i.e., resistance values above 126 Ω) recorded by the event detector.[17]

After completion of the test, a Weibull analysis was used to find the mean life of the inductors. The mean time to failure of the inductors in the accelerated test was found to be 62 cycles. A failure analysis was carried out on the failed PCB to determine whether the solder joints had really cracked. Two of the inductors showed visible cracks. Fig. 12 shows a crack in one of the center inductors. From the test, we see that the methodology predicted 52 cycles in temperature cycling for the inductors, while the mean time to failure in the actual accelerated test was 62 cycles.

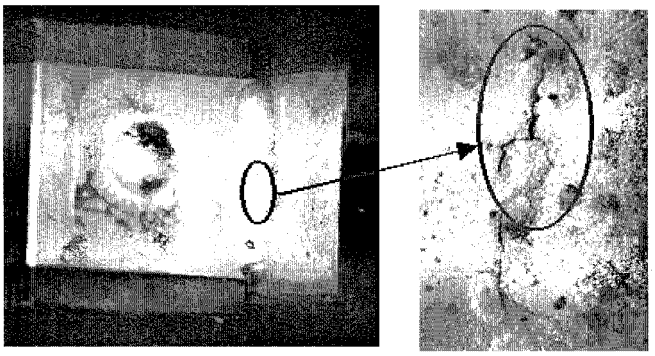

Fig. 12. Crack at the knee of the solder joint was observed on two inductors. The figure on the left shows the crack location. The solder joint crack is visible on the surface (figure on the right).

TABLE I
RESULT SUMMARY

	From calcePWA	From experiment
Cycles to failure for a new board only in thermal cycling	111	117
Cycles to failure expected for the board used in the experiment (0.468 remaining life fraction)	52	-
Actual cycles to failure for board used in the experiment	-	62
Remaining life fraction	0.47	0.53

After the completion of the test, a second accelerated test was carried out to find the life of an undamaged board. The mean time to failure of the board was 117 cycles, which corresponds to a remaining life fraction of 0.53 as calculated from experiment. This corresponds to an error of 13% from the value predicted by calcePWA (0.47—see Table I).

IV. CONCLUSION

This paper describes a practical methodology for life consumption monitoring, consisting of monitoring life cycle environment parameters, data simplification, and physics-of-failure analysis. The methodology was demonstrated by measuring real-time data and applying it to a test board using a commercially available reliability assessment software. An accelerated test was performed to verify the results of the life consumption analysis. The results show that the life consumption monitoring methodology can be used to determine the remaining life in a part for a given set of environmental and operating conditions.

[14]The displacement plot from the damage analysis closely matches the displacement plot for the first mode of vibration of the PCB, which is expected since the excitation frequency with the largest PSD lies close to the first natural frequency of the PCB.

[15]87.6% of the total damage was due to vibration and 12.3% of the total damage was due to temperature cycling.

[16]The choice of the accelerated test was not influenced by the real-life test. Temperature cycling was chosen simply because of chamber availability and ease of modeling. The temperature limits for the thermal cycling experiment were derived from the measured underhood environment, but the frequency of cycling was faster.

[17]The average resistance of the inductors before the accelerated test was 12.6 Ω, so we defined an "open" across the inductors as 10 times this value. The event detector we used can record up to 15 such events, so we chose 15 as our event counter.

REFERENCES

[1] B. K. N. Rao, *Handbook of Condition Monitoring*. Oxford, U.K.: Elsevier, 1996, pp. 1–12.
[2] "ETOPS Maintenance," *Aero Mag.*, no. 7, July 1999.
[3] M. Pecht, M. Dube, M. Natishan, and I. Knowles, "An evaluation of built-in test," *IEEE Trans. Aerosp. Electron. Syst.*, vol. 37, no. 1, pp. 266–272, Jan. 2001.
[4] N. Kelkar, A. Dasgupta, M. Pecht, I. Knowles, M. Hawley, and D. Jennings, ""Smart" electronic systems for condition-based health management," *Qual. Rel. Eng. Int.*, vol. 13, no. 1, pp. 3–8, Jan.–Feb. 1997.

[5] A. Ramakrishnan, T. Syrus, and M. Pecht, "Electronic hardware reliability," in *The Modern Microwave and RF Handbook*. Boca Raton, FL: CRC Press, 2000, pp. 3-102–3-121.
[6] J. J. Carr, *Sensors and Circuits*. Englewood Cliffs, NJ: Prentice-Hall, 1993, pp. 5–8.
[7] H. O. Fuchs, D. V. Nelson, M. A. Burke, and T. L. Toomay, "Shortcuts in cumulative damage analysis," in *Fatigue Under Complex Loading: Analyses and Experiments*, R. M. Wetzel, Ed. Warrendale, PA: SAE, 1977.
[8] L. Tucker, S. Downing, and L. Camillo, "Accuracy of simplified fatigue prediction methods," in *Fatigue Under Complex Loading: Analyses and Experiments*, R. M. Wetzel, Ed. Warrendale, PA: SAE, 1977.
[9] J. Collins, *Failure of Materials in Mechanical Design*. New York: Wiley, 1993.
[10] D. Socie, "Rainflow cycle counting: A historical perspective," in *The Rainflow Method in Fatigue*. Oxford, U.K.: Butterworth-Heinemann, 1991, pp. 3–10.
[11] K. D. Cluff, "Characterizing the commercial avionics thermal environment for field reliability assessment," *J. Inst. Environ. Sci.*, vol. 40, no. 4, pp. 22–28, Jul.–Aug. 1997.
[12] H. Anzai, "Algorithm of the rainflow method," in *The Rainflow Method in Fatigue*. Oxford, U.K.: Butterworth-Heinemann, 1991, pp. 11–20.
[13] M. A. Miner, "Cumulative damage in fatigue," *J. Appl. Mech.*, pp. A-159–A-164, Sept. 1945.
[14] W. J. Crichlow, A. J. McCulloch, L. Young, and M. A. Melcon, "An engineering evaluation of methods for the prediction of fatigue life in airframe structures," Flight Dynamics Lab., OH, Tech. Rep., ASD-TR-61-434, 1962.
[15] H. Azzam, "A practical approach for the indirect prediction of structural fatigue from measured flight parameters," in *Aircraft Health and Usage Monitoring Systems*. Suffolk, U.K.: Institution of Mechanical Engineers, 1996.
[16] *Saver User's Manual*, Dallas Instruments, Dallas, TX, 2000.
[17] J. H. Lau and Y. Pao, *Solder Joint Reliability of BGA, Flip Chip, and Fine Pitch SMT Assemblies*. New York: McGraw-Hill, 1997.
[18] S. J. Bendat and A. G. Piersol, *Random Data: Analysis and Measurement Procedures*. New York: Wiley, 1971.
[19] W. H. Press, S. A. Teukolsky, W. T. Vetterling, and B. P. Flannery, "The fast fourier transform," in *Numerical Recipes in C: The Art of Scientific Computing*. New York: Cambridge University Press, 1992, p. 505.

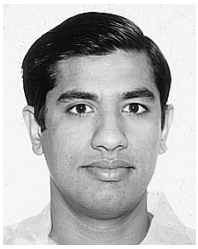

Arun Ramakrishnan received the M.S. degree in mechanical engineering from the University of Maryland, College Park. His thesis focused on life consumption monitoring, digital data collection and analysis, and sensor technologies.

His current job focus is on flip chip substrate design and characterization. He is a Package Development Engineer in LSI Logic Corporation, Milpitas, CA.

Michael G. Pecht (F'92) received the B.S. degree in acoustics, the M.S. degree in engineering, and the M.S. and Ph.D. degrees in engineering mechanics, all from the University of Wisconsin, Madison.

He is the Director of the CALCE Electronic Products and Systems Center, University of Maryland, College Park, and a Full Professor with a three-way joint appointment in mechanical engineering, engineering research, and systems research. He serves on the Board of Advisors for various companies and consults for the U.S. government, providing expertise in strategic planning in the area of electronics products development and marketing.

Dr. Pecht is an ASME Fellow. He served as Chief Editor of the IEEE TRANSACTIONS ON RELIABILITY for eight years and on the Advisory Board of IEEE SPECTRUM. He is currently the Chief Editor for *Microelectronics Reliability*, an Associate Editor for the IEEE TRANSACTIONS ON COMPONENTS AND PACKAGING TECHNOLOGIES, and on the Advisory Board of the *Journal of Electronics Manufacturing*.